Cilt 12, Sayı 1, Sayfa 44-52, 2023 Volume 12, Issue 1, Page 44-52, 2023

Araştırma Makalesi https://doi.org/10.46810/tdfd.1219070 Research Article

Türk Doğa ve Fen Dergisi
Turkish Journal of Nature and Science
www.dergipark.gov.tr/tdfd

Rapid Suppression of Superconductivity in Co_3O_4 Nanoparticles-added Bi-2212 Ceramics

Mehmet GÜRSUL[1*]

[1] Çukurova University, Faculty of Sciences and Arts, Department of Physics, Adana, Türkiye
Mehmet GÜRSUL ORCID No: 0000-0002-3025-2183

Corresponding author: mgursul@cu.edu.tr

(Received: 14.12.2022, Accepted: 15.02.2023, Online Publication: 27.03.2023)

Keywords
HTSCs,
XRD,
SEM,
Magnetic Hysteresis,
Critical Current Density

Abstract: This study concerns the remarkable variations in the crystalline quality, phase compositions, superconducting properties, and pinning force in the Bi-2212 ceramics through the addition of Co_3O_4 nano-particles with the x % weight for x = 0, 0.5, 1, and 2, respectively. From XRD analysis, it is deduced that Co_3O_4-inclusions give rise to the XRD peaks to expand, degrade the crystal quality together with a decrement in the Bi-2212 amount. From SEM images, it is seen that there is an evolution from rod-like structure to plate-like structure with Co_3O_4 addition. The critical transition temperature (T_c) value which is determined from *M-T* measurement is 82 K in the pure sample, it drops gradually and takes the value 65 K and 42 K for the 0.5% Co sample and 1% Co sample respectively, and eventually, the superconductivity is lost in the 2% Co sample. From *M-H* measurements, it is clear that the hysteresis loop gets narrower with Co_3O_4 addition and temperature. Accordingly, critical current densities (J_c) and pinning forces (F_p) reduce due to deteriorations in the connectivity between superconducting grains induced by the augmentation in Co_3O_4 content.

Co_3O_4 Nanoparçacıklarıyla Ekli Bi-2212 Seramiklerinde Süperiletkenliğin Hızlı Bastırılması

Anahtar Kelimeler
HTSCs,
XRD,
SEM,
Manyetik Histerezis,
Kritik Akım Yoğunluğu

Öz: Bu çalışma, sırasıyla x = 0, 0.5, 1 ve 2 için % x ağırlıkça Co_3O_4 nano-parçacıklarıyla eklenmiş Bi-2212 seramiğindeki kristal kalitesi, faz bileşimleri, süperiletken özellikler ve çivileme kuvvetindeki dikkate değer değişimlerle ilgilidir. XRD analizinden Co_3O_4-içeriğinin XRD piklerinde genişlemeye, kristal kalitesinin düşmesine ve Bi-2212 miktarının azalmasına yol açtığı sonucuna varılır. SEM görüntülerinden Co_3O_4 ilavesiyle çubuksu yapıdan plakamsı yapıya doğru bir evrilme olduğu görülmektedir. Kritik geçiş sıcaklığı (T_c), *M-T* ölçümlerinden saf örnekte 82 K olarak bulunmuş ve % 0.5 Co örneğinde 65 K'ye % 1 Co örneğinde 42 K'ye kademeli olarak düştükten sonra süperiletkenlik % 2 Co örneğinde kaybolmuştur. *M-H* ölçümlerinden, histerezis eğrilerinin Co_3O_4 eklenmesi ve sıcaklıkla birlikte daraldığı görülmektedir. Buna bağlı olarak, kritik akım yoğunlukları (J_c) ve çivileme kuvvetleri (F_p), Co_3O_4 içeriğindeki artışın neden olduğu süper iletken tanecikler arasındaki bağlantıdaki bozulmalar nedeniyle azalmıştır.

1. INTRODUCTION

The superconductivity was revitalized in 1986 thanks to the discovery of superconductivity in the copper-oxide based Ba−La−Cu−O system by Bednorz and Muller [1]. Prior to this progress, superconductivity was seen as a subject confined to temperatures near absolute zero and well explained by Bardeen–Cooper–Schrieffer (BCS) theory based on the electron-phonon interaction with a limit of critical transition temperature (T_c) of around 30 K [2]. However, after this discovery, superconductor studies accelerated tremendously and various high-T_c superconductors (HTSCs) such as Y-Ba-Cu-O (YBCO, T_c=90K) [3], Bi-Sr-Ca-Cu-O (BSCCO, T_c=110K) [4], and Tl–Ca/Ba–Cu–O (TBCCO, T_c= 120 K) [5] emerged within a year. What makes these discoveries important is that the critical temperature values are above the boiling point (77 K) of liquid nitrogen, which is accepted as the psychological and technological barrier of superconductivity. Among these high temperature superconductors, the BSSCO system is one of the most studied one and is represented by the general formula $Bi_2Sr_2Ca_{n-1}Cu_nO_{2n+4+y}$. This system has Bi-2201 (n=1), Bi-2212 (n=2), and Bi-2223 (n=3) phases, depending on the value of n, which shows the number of CuO_2 layers in the unit cell. As the CuO_2 layer in the structure increases, T_c values increase and are 20, 85 and 110 K for Bi-2201, Bi-2212, and Bi-2223, respectively [6]. Although the Bi-2201 phase without Ca was discovered first and led to the emergence of Bi-2212 and Bi-2223, it does not attract attention due to its low T_c. On the other hand Bi-2212 has attracted much attention due to its lesser weak link problems, lower fabrication cost, much easier manufacturability, and better thermodynamic stability compared to the Bi-2223 [7-8].

Since the discovery of BSCCO [9], chemical doping, which can be in the form of addition or substitution, has become one of the most used methods to enhance T_c and critical current density (J_c) or to uncover its physical and magnetic properties [10-16]. In addition to chemical doping, many synthesis routes are available to produce BSCCO bulk materials including solid state reaction [17], co-precipitation [18], sol-gel [19], and polymer matrix method [20]. Among these aforementioned methods, solid state one is frequently used by researchers owing to its advantages such as simplicity, cheapness, and reasonable reproducibility [14].

When a magnetic field applied to a Type-II superconductor is larger than the lower critical field (H_{c1}) and less than the upper magnetic field (H_{c2}), the superconductor exhibits a state called a mixed state (also known as vortex state or Shubnikov phase) where the magnetic field penetrates the superconductor in the configuration of quantized magnetic vortices carrying the magnetic flux quantum (ϕ_0). When a current density ($\boldsymbol{J}$) is applied to the material, a Lorentz force ($\boldsymbol{F}_L$= (1/c) $\boldsymbol{J} \times \phi_0$) emerges causing resistance by forcing vortices to move. The tools that struggle with the Lorentz force in the material are expressed as pinning centers. A pinning center can be formed naturally by defects such as stack faults, dislocations, and twin planes, or it can be constructed artificially via chemical doping or neutron radiation [21-22]. Basically, chemical doping attracts a lot of attention as it is an easy-to-control, non-destructive and effective method of producing pinning centers [23]. Doping of nano-sized particles to the BSCCO system has been proposed as a workable approach and many nanoparticles such as MgO [24], Al_2O_3 [25], ZrO_2 [26], Fe_3O_4 [27], and $NiFe_2O_4$ [28] have been tested.

In the current work, it is aimed to investigate the effect of Co_3O_4 nano-particles on the structural, superconducting, and magnetic properties of Bi-2212. Parenthetically, Co_3O_4 nanoparticles have multifunctional properties and are used in many applied areas such as energy storage [29], resistive switching devices [30], and biomedical technologies [31]. Co_3O_4 is an intrinsic antiferromagnetic material having a Neel temperature of 40 K with weak ferromagnetic behavior due to the presence of both Co^{2+} and Co^{3+} cations and uncompensated surface spins or finite size effect [32]. Considering these multifunctional properties of Co_3O_4, it will be interesting to test whether Co_3O_4 nanoparticles have the capability to form effective pinning centers in BSCCO. In this regard, Co_3O_4 nanoparticles were produced using sol-gel auto combustion method described in detail elsewhere [33, 34] and added to Bi-2212 for different weights. Characterizations of the prepared samples were performed with conventional methods, viz., X-ray diffraction (XRD), scanning electron microscope (SEM), magnetization-temperature, and magnetic hysteresis techniques.

2. MATERIAL AND METHOD

$Bi_2Sr_2Ca_1Cu_2O_y$+x % weight for x=0, 0.5, 1, and 2 % polycrystalline specimens were synthesized from the high purity commercial powders of Bi_2O_3, $SrCO_3$, $CaCO_3$, and CuO via the standard solid state reaction technique. These starting powders are exactly weighted in the molar proportion by an electronic balance and are well mixed and milled. Then, the resultant mixture was calcined twice for 12 h at 750°C and 800°C together with intermediate grinding in an agate mortar using a pestle for about 25 min. After the calcination process, the obtained homogenous powders were pressed into tablets with 0.9 mm thick and 0.5 cm in diameter applying pressure of 5000 kg-force/cm^2 at room temperature. Then these pressed samples are sintered at 860°C for 60 h followed by cooling to 800°C and quenching to room temperature in air to provide a large amount of Bi-2212 phase. After this heat treatment process, Co_3O_4 nanoparticles obtained by sol-gel auto-combustion method corresponding to the x% weight of Bi-2212 was added to the specimens and the thermal treatment steps described above were carried out once more and finally, all samples were made ready for the characterization process. Throughout the paper, the prepared samples with nominal ratios of $Bi_2Sr_2Ca_1Cu_2O_y$+ x weight % Co_3O_4 where x= 0, 0.5, 1, and 2 % are named as 0 % Co, 0.5 % Co, 1 % Co, and 2 % Co, respectively. As for XRD analysis, PANalytical Empyrean diffractometer with Cu-Kα target (λ= 1.54 Å) was used at room temperature. Microstructural features of the samples were investigated by FEI-Quanta FEG 650 SEM. The magnetic measurements namely magnetization as a function of temperature (*M-T*) and magnetization versus magnetic field (*M-H*) were conducted using a 7304 model Lake Shore VSM system.

3. RESULTS AND DISCUSSION

Figure 1 represents XRD patterns between 20 and 50° at room temperature of the pristine and Co_3O_4 added Bi-2212 ceramics. Most of the diffractions peaks can be indexed to Bi-2201, Bi-2212, and Bi2223 labeled by 1, 2 and 3, respectively. In addition to these peaks secondary phases shown by asterisk are also observed in all samples. Although these peaks are not Co_3O_4 peaks, they have not been clearly defined and probably belong to non-superconducting phases such as $CaCuO_2$ or $CaBi_2O_4$ combined with Co_3O_4. To make a quantitative analysis, the relative phase abundance of each phase can be calculated by the equations given below;

$$f_{2212} = \frac{\sum I_{2212}}{\sum I_{2223} + \sum I_{2212} + \sum I_{2201} + \sum I_{other}} \times 100\% \quad (2)$$

$$f_{2201} = \frac{\sum I_{2201}}{\sum I_{2223} + \sum I_{2212} + \sum I_{2201} + \sum I_{other}} \times 100\% \quad (3)$$

$$f_{other} = \frac{\sum I_{other}}{\sum I_{2223} + \sum I_{2212} + \sum I_{2201} + \sum I_{other}} \times 100\% \quad (4)$$

where *f* is the phase percentage and *I* corresponds to the peak intensity of the related phase [6]. According to calculations embedded in Table 1, a considerable decrease in superconducting phases with the introduction of Co_3O_4. In particular, the amount of the Bi-2212 phase decreases from 74.4 to 46.6 % with only 2% Co_3O_4 addition. Besides, the Bi-2223 phase, which was around 8.5 % in the pure sample, completely disappeared in the 2% Co_3O_4-added sample. In addition, the Bi-2201 phase, which is around 11-12% in other samples, reached its smallest value of 9.2% in the 2% Co sample. More interestingly, non-superconducting secondary phases increased dramatically with the increase in Co_3O_4, taking a value of 44.2 % in the 2% Co sample. It should also be stated that the inclusions of Co_3O_4 in the system caused the XRD peaks to expand, reduce the crystal quality of the structure and thereby undermine the growth of the Bi-2212 phase. Moreover, observed peaks can be assigned to the tetragonal structure with space group $P_{4/mmm}$ and cell parameters can be determined through the equation [12]:

$$\frac{1}{d^2} = \frac{h^2}{a^2} + \frac{k^2}{b^2} + \frac{l^2}{c^2} \quad (5)$$

where d is the interlayer distance, h, k, and l are the Miller indices and a, b, and c are the lattice constants. As seen from the obtained values provided in Table 1, both a and c parameters reduce with Co_3O_4 addition; however, the decrease in c is more pronounced. The shrinkage of c cell germinates from the variation in the stability of oxygen level in the Bi-O stacks owing to the charge neutrality mechanism [6]. Furthermore, the average crystallite size of the samples can be deduced using Debye-Scherrer equation given as [35];

$$L = \frac{0.941\,\lambda}{\beta\,\cos\theta_\beta} \quad (6)$$

where L is the crystallite-size, λ the X-ray wavelength used in the diffractometer, β is the full width at half maximum of the peak, and θ_β is the Bragg diffraction angle. The most intense peaks around 23.03°, 24.85°, 27.41°, 30.94°, and 33.11° corresponding to planes of

$$f_{2223} = \frac{\sum I_{2223}}{\sum I_{2223} + \sum I_{2212} + \sum I_{2201} + \sum I_{other}} \times 100\% \quad (1)$$

(008), (013), (015), (017), and (110) are used in the estimation of the average crystallite size. As clear from Table 2, the average crystallite size declines monotonically with the increment in Co_3O_4-content in Bi-2212 reflecting that Co_3O_4 additions scupper crystallinity of the Bi-2212. Put succinctly, Co_3O_4 inclusions raise the crystallization activation energy (E_a) of the Bi-2212 phase and expedite the nucleation rates of the secondary phases [36].

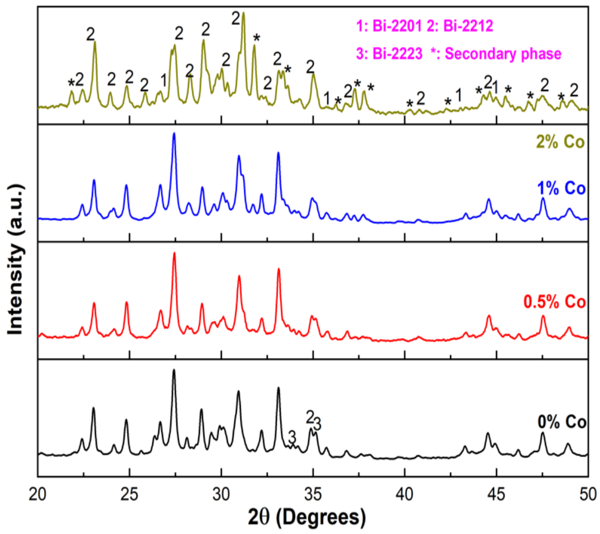

Figure 1. XRD patterns of Co_3O_4 nanoparticles-added Bi-2212 ceramics

The morphological properties of the samples were examined with SEM images taken at 1000X magnification in the secondary electron mode and obtained photographs are given in Figure 2. In the light of the first browses made to the photographs, it is seen that the addition of Co_3O_4 % significantly changes crystallinity and morphological characteristics of the samples. Namely, if one pays attention to the images in the pure sample (Figure 2a), while the rod- and needle-like grains constitute the microstructure forming a tight union by contacting each other, these structures have decreased in the Co_3O_4–added samples and the flaky structures and plate-like structures have emerged due to the expansion in the melting regions. The added Co_3O_4 accumulates at the boundaries of these rod-like grains forming the Bi-2212 structure causing the formation of melt regions in the structure, impairing the crystal quality, and breaking the connection between the superconducting grains. These variations in the morphological properties of the samples can be correlated with the serious decrement in the Bi-2212 percentages addressed in XRD discussions.

Table 1. Phase fractions and lattice parameters of the samples

Sample	Bi-2223 %	Bi-2212 %	Bi-2201 %	Other %	a (Å)	c (Å)
%0 Co	8.5	74.4	11.1	6.0	5.4093	30.8879
%0.5 Co	6.2	68.8	12.1	12.9	5.4061	30.8444
%1 Co	2.8	64.0	12.1	21.1	5.4082	30.8442
%2 Co	0.0	46.6	9.2	44.2	5.3781	30.7945

Table 2. Determination of average crystallite size estimated from the Debye-Scherrer relation using the reflections at 2θ= 23.03°, 24.85° 27.41°, 30.94°, and 33.11°

2θ (Degrees)	0% Co (nm)	0.5% Co (nm)	1% Co (nm)	2% Co (nm)
23.03	56.99	52.54	53.67	53.41
24.85	51.41	60.42	52.55	47.80
27.41	68.19	42.24	45.16	51.65
30.94	52.41	46.06	46.86	44.04
33.11	67.98	64.11	61.08	15.75
Average Crys.Size (L)	59.40	53.07	51.86	42.53

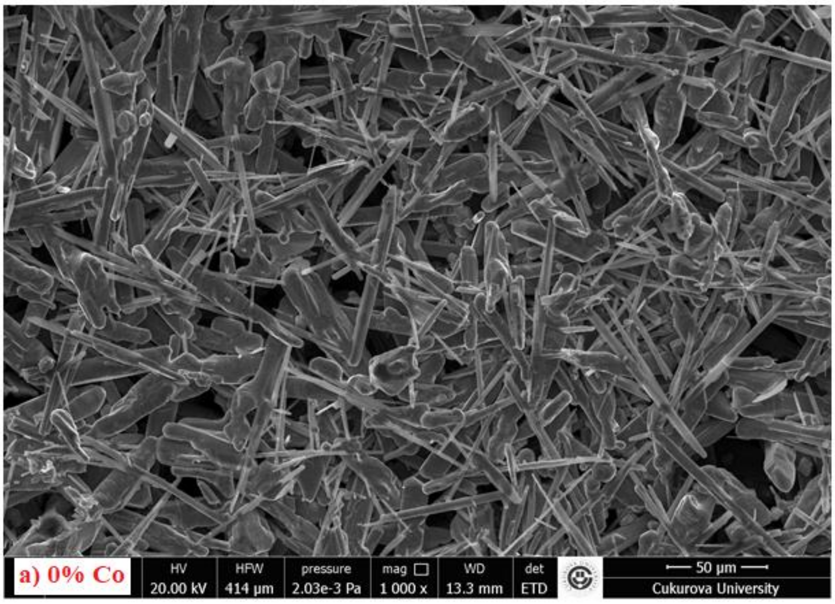

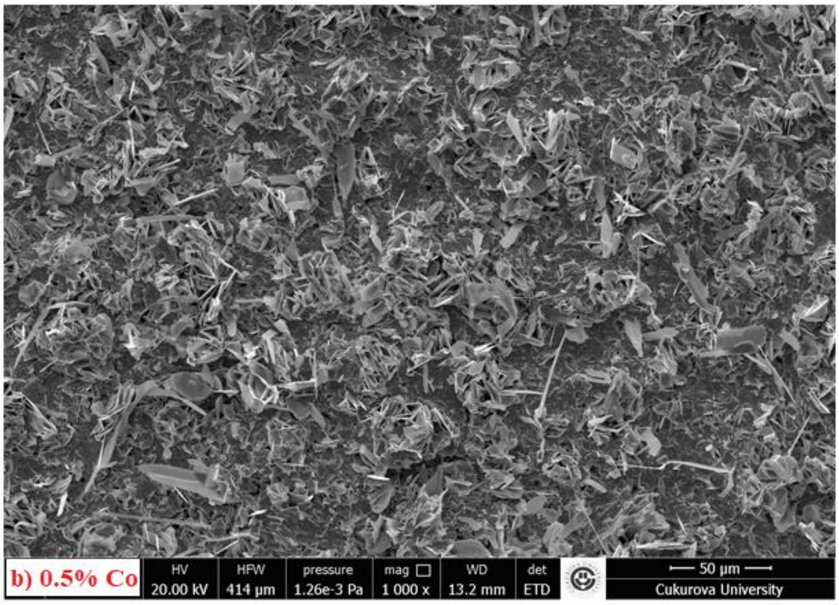

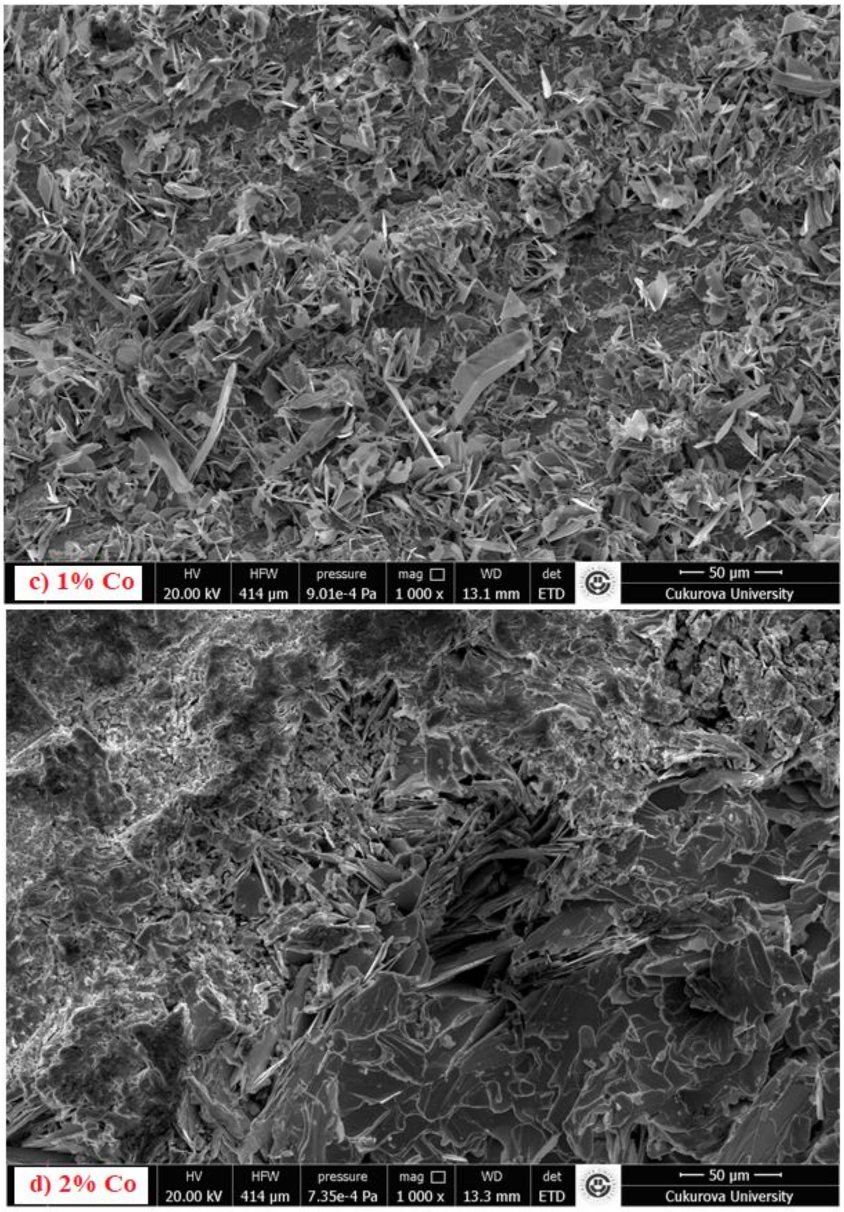

Figure 2. SEM images for a) 0% Co, b) 0.5% Co, c) 1% Co and, d) 2% Co samples

Magnetization versus temperature curves at the applied field of 100 Oe is given in Figure 3. The transition temperature (T_c) which corresponds to beginning point of diamagnetic signals decreases harshly with the addition of Co_3O_4. To put it numerically, the T_c value in the pure sample is 82 K, while in the 0.5% Co sample it drops sharply, takes the value 65 K. The critical temperature value reduces to 42 K in the 1% sample and the superconductivity is lost in the 2% sample. This dramatic decrease in T_c values can be elucidated within the framework of the pair-breaking theory suggested by Abrikosov and Gor'kov [37, 38]. Namely, as a consequence of the interaction of the electrons of the magnetic impurities and the Cooper pairs, the spins of the electrons change and the Cooper-pairs breakage occurs. More specifically, the significant decrease in T_c values is associated with the increase of the Gennes factor ($G=(g-1)^2 J (J+1)$), including Lande g factor and the total angular momentum due to magnetic impurities [38]. According to the Abrikosov-Gor'kov theory [37] the reduction of T_c values due to magnetic impurities is given by the relation;

$$\ln\frac{T_{c0}}{T_c} = \psi\left[\frac{1}{2}+\frac{\Gamma}{2\pi k_B T_C}\right] - \psi\left[\frac{1}{2}\right] \quad (7)$$

where T_{c0} is the transition temperature of the pure material (without magnetic impurity), ψ is the digamma function, and Γ is the pair-breaking parameter proportional to the magnetic impurity concentration [39]. If we relate to our case, it can be said that the Co_3O_4-impurities gradually actualize pair-breaking in Bi-2212 leading to a decrement in T_c values. However it can be emphasized that doping with non-magnetic impurities in cuprates can also degrade their T_c as in the case of Zn-doped [40] or Y-doped BSCCO [41]. The vanquishing of superconductivity in the non-magnetic impurity containing BSCCO can be expounded that random impurity potentials evolve due to enhancement of nonmagnetic disorder leading to the localization of electronic states at the Fermi level [39, 41, 42]. Hence another scenario of the rapid decrement in T_c is the result of new permanent crystallinity disorders such as porosity, defects, cracks, and grain boundary coupling problems evolving with the addition of Co_3O_4 [6]. Eventually, 2% Co doping level exterminate the superconductivity in Bi-2212 system resulting in a metal-insulator type transition (MIT) [40, 43].

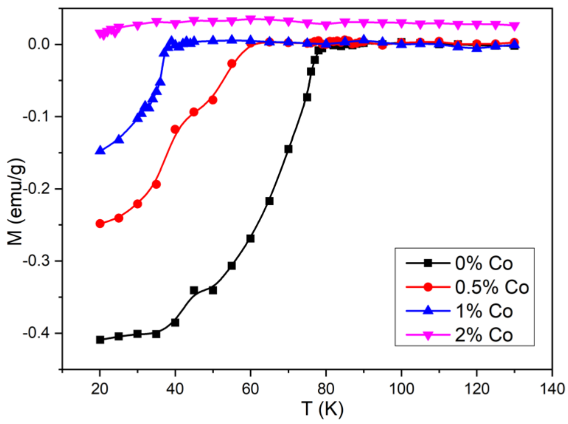

Figure 3. Magnetization versus temperature curves of the samples.

Magnetic field dependence of magnetization of the samples (M-H) measured at 10, 15, and 20 K between $\pm$ 1 T are illustrated in Figure 4. It is clear that the area of the magnetic hysteresis gets narrower with addition of Co_3O_4 and with increasing temperature. This is stem from the fact that the addition of Co_3O_4 and increasing temperature reduce the pinning ability of Bi-2212. Similarly, H_{c1} values for the samples where magnetization-magnetic field curves deviate from linearity and vortices emerge show a decreasing trend as Co_3O_4 enters the system. For example, H_{c1} of the pure sample at 10 K is 1611 Oe, while H_{c1} of the 1% Co sample decreases to 1242 Oe. In addition, M_r values which we call remanent magnetization and represent the flux trapping in the system decreased with increasing amount of Co_3O_4. The change of H_{c1} and M_r values are given in Table 3 for different Co_3O_4-content at temperatures of 10, 15 and 20 K, respectively.

Using magnetization versus magnetic field data, the intra-grain critical current densities, J_c, in A/cm^2, of all samples can be calculated using Bean's model given as [44,45];

$$J_c = 20\Delta M/[a(1-a/3b)] \tag{8}$$

where ΔM is the difference between the magnetization values of up and down fields measured in emu/cm^3 and, a and b (a<b) are the dimensions of the samples. Obtained J_c values of the samples are depicted in Figure 5 for temperatures of 10, 15, and 20 K. It can be seen from the graphs that the negativity on the superconducting properties with Co_3O_4 is also reflected in the critical current densities decreased significantly with the increasing amount of Co_3O_4. As the amount of Co_3O_4 rises, the amount of the Bi-2212 phase reduces and the connectivity of superconducting grains weakens, causing serious drops in the critical current densities of the samples.

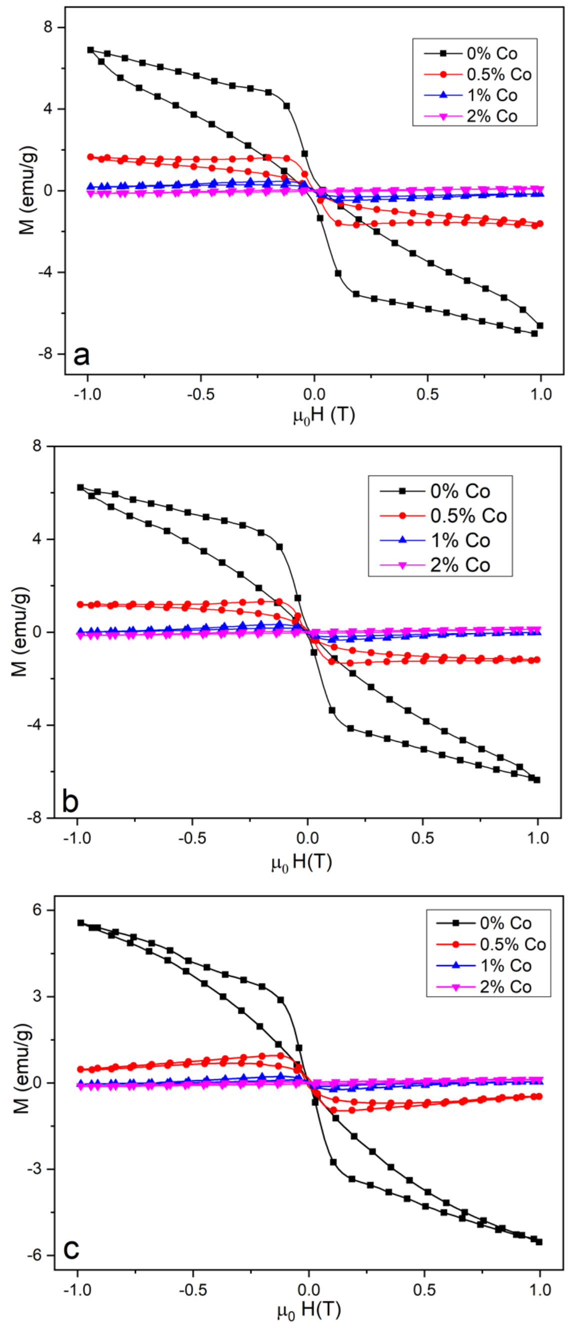

Figure 4. Magnetization versus magnetic field for a) 10 K, b) 15 K, and c) 20 K

As the final calculation, the volume pinning force (F_p) of the samples can be determined using the equation below [45].

$$F_P = J_C \times B \tag{9}$$

Calculated F_p values as a function of the magnetic field for all samples are given in Figure 6. If the figure is examined, it can be deduced that F_P values decline with increasing temperature and Co_3O_4-content. The maximum F_p was calculated to be approximately 4.2 × 10^6 N/m^3 in the pristine sample at 10 K. However with the increment in Co_3O_4, this value reduces to 0.8 × 10^6 in 0.5% Co_3O_4 sample for the applied field of 0.8 T.

All in all, it can be deduced that introducing Co_3O_4 nanoparticles to the Bi-2212 superconductor undermines the pinning ability of the superconductor.

Table 3. H_{c1} and M_r values of the samples at 10, 15, and 20 K.

Sample	H_{c1} (Oe) at 10 K	M_r (emu/gr) at 10 K	H_{c1} (Oe) at 15 K	M_r (emu/gr) at 15 K	H_{c1} (Oe) at 20 K	M_r (emu/gr) at 20 K
0% Co	1611	0.560	1478	0.750	1305	0.025
0.5% Co	1376	0.041	1297	0.023	1112	~0
1% Co	1242	0.027	1141	0.009	1065	~0
2%Co	~0	~0	~0	~0	~0	~0

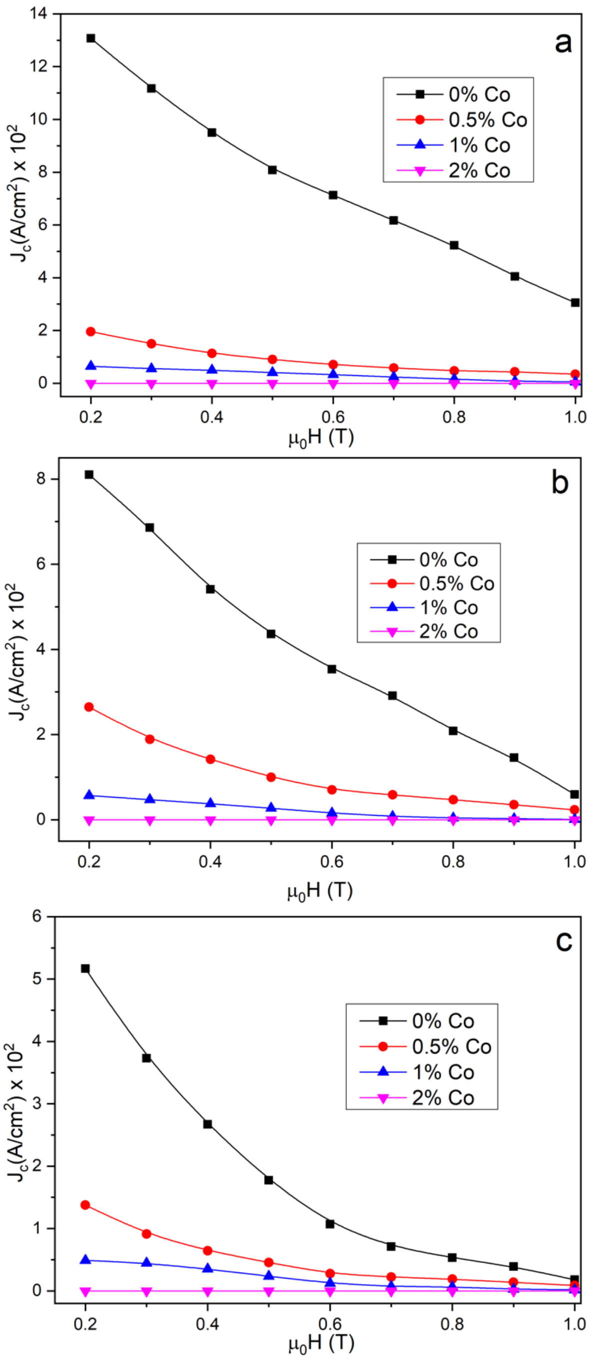

Figure 5. Critical current density versus magnetic field for a) 10 K, b) 15 K, and c) 20 K

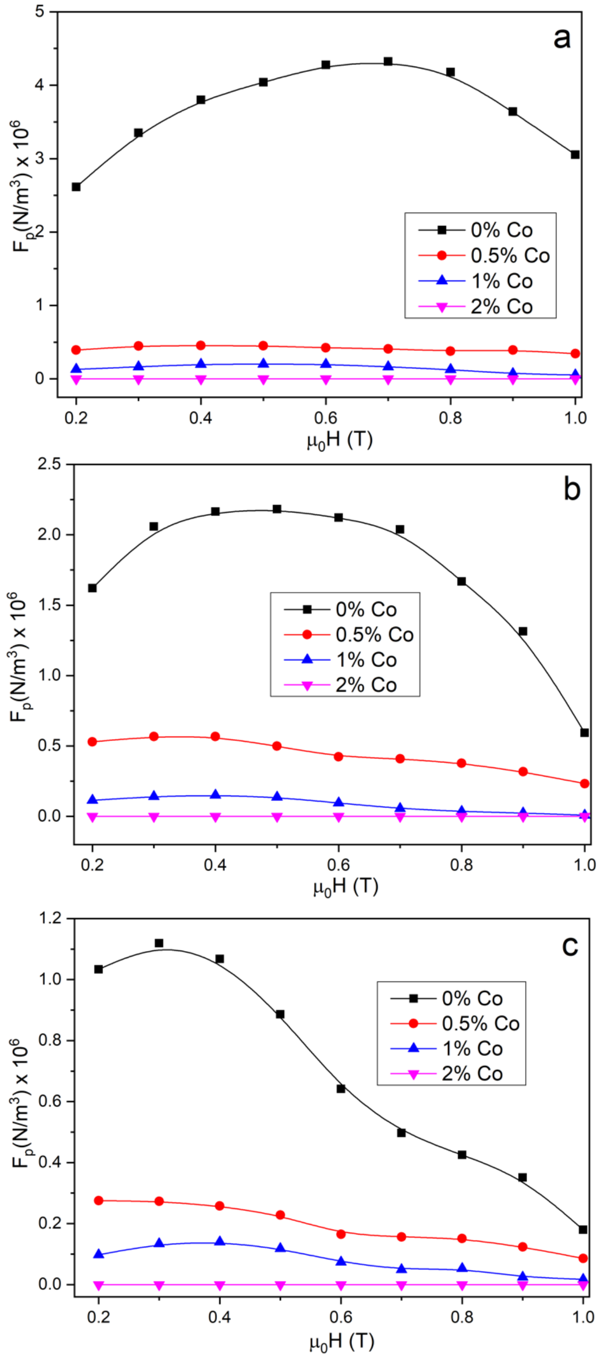

Figure 6. Variation of pinning force against magnetic field for a) 10 K, b) 15 K, and c) 20 K

4. CONCLUSION

In the current study, the influence of Co_3O_4-nanoparticle addition on the phase distributions including Bi-2201, Bi-2212, and Bi-2223, average crystallite size, morphological and microstructural features, superconducting and magnetic hysteresis properties of $Bi_2Sr_2CaCu_2O_y$ + x wt % Co_3O_4 (x=0, 0.5, 1, 2) ceramics prepared by classical solid state reaction technique are investigated with the aid of XRD, SEM, magnetization-temperature, and magnetization-magnetic field experiments. XRD surveys reveal that Bi-2212 phase reduces considerably and some non-superconducting secondary phases prominently enhance with the introducing of Co_3O_4. Besides, it can be detected from the SEM images that there is a transformation from rod-like structure to plate-like structure in the microstructure with Co_3O_4-content. From *M-T*, it seems that there is a rapid reduction in T_c values due to pair-breaking effect and localization of charge carriers through Co_3O_4 doping. From *M-H*, it is evident that hysteresis loop gets narrower with Co_3O_4 addition and temperature. In relation to this, M_r value at 10 K representing flux pinning ability of the samples is 0.560 emu/gr for 0% Co sample and harshly drops to 0.027 emu/gr in 1% Co sample. Moreover, it is determined that critical current densities (J_c) and pinning forces (F_p) of the samples also reduce as a consequence escalation of structural problems and weakening of the connectivity between the superconducting clusters induced by Co_3O_4-doping. All in all, the discussions mentioned throughout the text plainly reveal that Co_3O_4 nanoparticles play an inhibitory role in creating effective pinning centers in Bi-2212 system.

Acknowledgement

The author expresses his deep gratitude to Prof. Dr. Bekir Özçelik for the valuable suggestions and discussions. The author dedicates this work to his children Furkan, Hakan and Ayça.

REFERENCES

[1] Bednorz J G, Müller K.A. Possible high Tc superconductivity in the Ba−La−Cu−O system. Z. Physik B - Condensed Matter. 1986; 64: 189–193.
[2] Bardeen J, Cooper L N., Schrieffer J R, Microscopic Theory of Superconductivity. Phys. Rev. 1957; 106: 162.
[3] Wu M K, Ashburn J R, Torng C J, Hor P H, Meng R. L., Gao L, Huang Z J, Wang Y Q, Chu C W, Superconductivity at 93 K in a new mixed-phase Y-Ba-Cu-O compound system at ambient pressure. Phys. Rev. Lett. 1987; 58: 908.
[4] Maeda H, Tanaka Y., Fukutomi M, Asano T, Togano K, Kumakura H, Uehara M, Ikeda S, Ogawa K, Horiuchi S, Matsui Y, New high-Tc superconductors without rare earth element. Physica C 1988; 153–155: 602–607.
[5] Sheng Z, Hermann A, Bulk superconductivity at 120 K in the Tl–Ca/Ba–Cu–O system. Nature. 1988; 332, 138–139.
[6] Ulgen A T, Yildirim G, Degradation in fundamental characteristic features of Bi-2212 superconducting ceramic material with Sr/Ti partial substitution. J Mater Sci: Mater Electron. 2019; 30: 8268–8277.
[7] Biju A , Aloysius R P , Syamaprasad U, Enhanced critical current density in Gd-added (Bi, Pb)-2212 bulk superconductor. Supercond. Sci. Technol. 2005; 18:1454-1459.
[8] Yildirim G, Determination of optimum diffusion annealing temperature for Au surface-layered Bi-2212 ceramics and dependence of transition temperatures on disorders, Journal of Alloys and Compounds. 2017; 699: 247-255.
[9] Maeda H, Tanaka Y, Fukutomi M, Asano T, A New High-Tc Oxide Superconductor without a Rare Earth Element Jpn. J. Appl. Phys. 27, L209.
[10] Biju A, Vinod K, Aloysius RP, Syamaprasad U, Improved superconducting properties by La addition in (Bi, Pb)-2212 bulk superconductor. J. Alloys Compd. 2007; 431: 49–55.
[11] Özçelik B, Gündoğmuş H, Yazıcı D, Effect of (Ta/Nb) co-doping on the magnetoresistivity and flux pinning energy of the BPSCCO superconductors. J Mater Sci: Mater Electron. 2014; 25: 2456–2462.
[12] Guner S B, Zalaoglu Y, Turgay T, Ozyurt O, Ulgen AT, Dogruer M, Yildirim G, A detailed research for determination of Bi/Ga partial substitution effect in Bi-2212 superconducting matrix on crucial characteristic features. Journal of Alloys and Compounds. 2019; 772: 388-398.
[13] Sedky A, Al-Battat W, Effect of Y substitution at Ca site on structural and superconducting properties of Bi:2212 superconductor. Physica B: Condensed Matter. 2013; 410: 227-232.
[14] Fallah-Arani H, Baghshahi S, Sedghi A, Stornaiuolo D, Tafuri F, Riahi-Noori N, Enhancement in superconducting properties of $Bi_2Sr_2Ca_1Cu_2O_{8+\theta}$ (Bi-2212) by means of boron oxide additive. Physica C: Superconductivity and its Applications. 2018; 548: 31-39.
[15] Ozabaci M, Sotelo A, Madre M.A, Yakinci M A, Effect of Fe Substitution for Cu on Microstructure and Magnetic Properties of Laser Floating Zone (LFZ) Grown Bi-2212 Rods. J Supercond Nov Magn 2013; 26: 1143–1149.
[16] Lu T., Zhang C, Guo S, Wu Y, Li C, Zhou L, The influence of critical current density of Bi-2212 superconductors by defects after Yb-doping, Physica C: Superconductivity and its Applications, 2015; 519:24-27.
[17] Türk N, Gündoğmuş H, Akyol M, Yakıncı Z D, Ekicibil A, Özçelik B, Effect of Tungsten (W) Substitution on the Physical Properties of Bi-(2223) Superconductors. J Supercond Nov Magn. 2014; 27: 711–716.
[18] Hamadneh I, Halim S A. Lee, C K, Characterization of $Bi_{1.6}Pb_{0.4}Sr_2Ca_2Cu_3O_y$ ceramic superconductor prepared via coprecipitation method at different sintering time. J Mater Sci. 2006; 41: 5526–5530.
[19] Li D., Zhang H, Gao X, Yang S, Chen Q, Effect of the fabrication process on the electrical properties of polycrystalline $Bi_{1.7}Pb_{0.3}Sr_2Ca_2Cu_3O_{10}$. Ceramics International. (2016) 42(1): 1728-1732.
[20] Gürsul M, Ekicibil A, Özçelik B, Sotelo A, Madre M A, Sintering Effects in Na-Substituted Bi-(2212) Superconductor Prepared by a Polymer Method. J Supercond Nov Magn 2015; 28: 1913–1924.

[21] Yazici D, Erdem M, Ozcelik B, Improvement of the Intergranular Pinning Energy in the $(BiPb)_2Sr_2Ca_2Cu_3O_{10+\delta}$ Superconductors Doped with High Valancy Cations. J Supercond Nov Magn. 2012; 25:725–729.

[22] Trastoy J, Rouco V, Ulysse C, Bernard R, Faini G, Lesueur J, Briatico J, Villegas J E, Nanostructuring of high-TC superconductors via masked ion irradiation for efficient ordered vortex pinning. Physica C 2014; 506:195-200.

[23] Boudjadja Y, Amira A, Saoudel A, Varilci A, Altintas S P, Terzioglu C, Structural and electrical properties of cerium doped Bi(Pb)-2212 phases. Physica B: Condensed Matter 2014; 443:130-135.

[24] Wei W, Schwartz J, Goretta K C, Balachandran U, Bhargava A, Effects of nanosize MgO additions to bulk $Bi_{2.1}Sr_{1.7}CaCu_2O_x$. Physica C: Superconductivity. 1998; 298(3-4): 279-288.

[25] Aftabi A, Mozaffari M, Intergranular Coupling, Critical Current Density, and Phase Formation Enhancement of Polycrystalline $Bi_{1.6}Pb_{0.4}Sr_2Ca_2Cu_3O_{10-y}$ Superconductors by α-Al_2O_3 Nanoparticle Addition. J Supercond Nov Magn. 2015; 28: 2337–2343.

[26] Zouaoui M, Ghattas A, Annabi M, Azzouz F B, Salem, M B, Effect of nano-size ZrO_2 addition on the flux pinning properties of (Bi, Pb)-2223 superconductor. Supercond. Sci. Technol. (2008); 21(12):125005.

[27] Abd-Shukor R, Kong W, Magnetic field dependent critical current density of Bi–Sr–Ca–Cu–O superconductor in bulk and tape form with addition of Fe_3O_4 magnetic nanoparticles. J. Appl. Phys. 2009; 105: 07E311.

[28] Kong W, Abd-Shukor R, Enhanced Electrical Transport Properties of Nano $NiFe_2O_4$-added $(Bi_{1.6}Pb_{0.4})Sr_2Ca_2Cu_3O_{10}$ Superconductor. J Supercond Nov Magn. 2010; 23:257.

[29] Liu Y, Mi C, Su L, Zhang X, Hydrothermal synthesis of Co_3O_4 microspheres as anode material for lithium-ion batteries, Electrochimica Acta, 2008; 53(5): 2507-2513.

[30] Younis A, Chu D, Lin X, Lee J, Li S, Bipolar resistive switching in p-type Co_3O_4 nanosheets prepared by electrochemical deposition. Nanoscale Res Lett. 2013; 8: 36.

[31] Santra S, Wang K, Tapec R, Tan W, Development of novel dye-doped silica nanoparticles for biomarker application. J. Biomed. Opt. 2001.

[32] Bindu Duvuru H, Alla S K, Shaw S K, Meena S S, Gupta N, Vara Prasad B.B.V.S., Kothawale M M, Kumar M K, Prasad N K, Magnetic and dielectric properties of Zn substituted cobalt oxide nanoparticles. Ceramics International. 2019; 45(13):16512-16520.

[33] Wicaksono Y A, Puspitasari P, Pratama M M A., A. Permanasari A, Sukarni S, Synthesis and characterisation of cobalt oxide (Co_3O_4) using sol-gel auto combustion method with stirring time variations. AIP Conference Proceedings. 2022; 2489:030031.

[34] Razavi F S, Sobhani A, Amiri O, Ghiyasiyan-Arani M, Salavati-Niasari M, Green sol-gel auto-combustion synthesis, characterization and investigation of the electrochemical hydrogen storage properties of barium cobalt oxide nanocomposites with maltose. International Journal of Hydrogen Energy. 2020; 45 (35): 17662-17670.

[35] Cullity B D, Element of X-ray Diffraction (Addition-Wesley, Reading, 1978).

[36] Dogruer M, Yildirim G, Terzioglu C, Evolution of electrical, superconducting, crystallinity and structural features with aliovalent Nd/Sr replacement in Bi-2223 ceramics. Materials Chemistry and Physics. 2022; 288: 126350.

[37] Abrikosov A A, Gor'kov L P, Contribution to the theory of superconducting alloys with paramagnetic impurities. Zh. Eksp. Teor. Fiz. 1960; 39:1781–1796.

[38] Zalaoglu Y, Yildirim G, Buyukuslu H, Saritekin N K, Varilci A, Terzioglu C, Gorur O, Important defeats on pinning of 2D pancake vortices in highly anisotropic Bi-2212 superconducting matrix with homovalent Bi/La substitution. Journal of Alloys and Compounds. 2015; 631: 111-119.

[39] Nkum R K, Punnett A, Datars W R, Substitution of 3d metals for Cu in $(Bi, Pb)_2Sr_2Ca_2Cu_3O_y$. Physica C. 1992: 20; 371-378.

[40] Maeda A, Yabe T, Takebayashi S, Hase M., Uchinokura K, Substitution of 3d metals for Cu in $Bi_2(Sr_{0.6}Ca_{0.4})_3Cu_2O_y$. Phys. Rev. B 1989; 41: 4112.

[41] Singh S, Suppression of superconductivity in Sm and Co substituted Bi Sr Ca Cu O system. Physica C. 1998; 294: 249–256.

[42] Jayaram B, Lanchester P C, Weller M T, Localization and interaction effects during superconductor-insulator transition of $Bi_2Sr_2Ca_{1-x}Gd_xCu_2O_{8+d}$, Phys. Rev. B 1991; 43: 5444.

[43] Yildirim G, Beginning point of metal to insulator transition for Bi-2223 superconducting matrix doped with Eu nanoparticles, Journal of Alloys and Compounds. 2013; 578: 526-535.

[44] Bean C P, Magnetization of Hard Superconductors. Phys. Rev. Lett. 1962; 8: 250.

[45] Gursul M, Ozcelik B, Liu M, Boltalin A I, Morozov I V, Structural and physical properties of Na-substituted $K_{0.8}Fe_{2-y}Se_2$ single crystal. Journal of Alloys and Compounds, 2019; 777: 1074-1079.